Journal of Catalysis 338 (2016) 82–93

Contents lists available at ScienceDirect

Journal of Catalysis

journal homepage: www.elsevier.com/locate/jcat

Redox mechanism for selective oxidation of ethanol over monolayer V_2O_5/TiO_2 catalysts

Vasily V. Kaichev [a,b,*], Yuriy A. Chesalov [a,b], Andrey A. Saraev [a,b], Alexander Yu. Klyushin [c,d], Axel Knop-Gericke [c], Tamara V. Andrushkevich [a], Valerii I. Bukhtiyarov [a,b]

[a] Boreskov Institute of Catalysis, Lavrentieva Ave. 5, 630090 Novosibirsk, Russia
[b] Novosibirsk State University, Pirogov Str. 2, 630090 Novosibirsk, Russia
[c] Department of Inorganic Chemistry, Fritz Haber Institute of the Max Plank Society, Faradayweg 4-6, D-14195 Berlin, Germany
[d] Helmholtz-Zentrum Berlin für Materialien und Energie GmbH, Division Energy Material, Albert-Einstein-Str. 15, 12489 Berlin, Germany

ARTICLE INFO

Article history:
Received 27 November 2015
Revised 16 February 2016
Accepted 18 February 2016

Keywords:
Heterogeneous catalysis
Ethanol oxidation
Acetaldehyde
Acetic acid
Vanadia

ABSTRACT

The selective oxidation of ethanol to acetaldehyde and acetic acid over a monolayer V_2O_5/TiO_2 catalyst has been studied in situ using Fourier transform infrared spectroscopy and near-ambient-pressure X-ray photoelectron spectroscopy (XPS) at temperatures ranging from 100 to 300 °C. The data were complemented with temperature-programmed reaction spectroscopy and kinetic measurements. It was found that under atmospheric pressure at low temperatures acetaldehyde is the major product formed with the selectivity of almost 100%. At higher temperatures, the reaction shifts toward acetic acid, and at 200 °C, its selectivity reaches 60%. Above 250 °C, unselective oxidation to CO and CO_2 becomes the dominant reaction. Infrared spectroscopy indicated that during the reaction at 100 °C, nondissociatively adsorbed molecules of ethanol, ethoxide species, and adsorbed acetaldehyde are on the catalyst surface, while at higher temperatures the surface is mainly covered with acetate species. According to the XPS data, titanium cations remain in the Ti^{4+} state, whereas V^{5+} cations undergo reversible reduction under reaction conditions. The presented data agree with the assumption that the selective oxidation of ethanol over vanadium oxide catalysts occurs at the redox V^{n+} sites via a redox mechanism involving the surface lattice oxygen species. A reaction scheme for the oxidation of ethanol over monolayer V_2O_5/TiO_2 catalysts is suggested.

1. Introduction

Over the past several years, the idea of using renewable resources in the chemical industry has become popular worldwide. In particular, a great many efforts have been made to develop technologies for the production of alternative fuels based on bio-oil, biodiesel, or bioethanol [1–4]. At the same time, bioethanol, or simply "ethanol," which is produced from biomass by hydrolysis and sugar fermentation processes, can be used as a raw material for catalytic production of various useful chemical compounds. Depending on the catalyst and reaction conditions, ethanol can be transformed to acetaldehyde, acetic acid, butanol, or ethyl acetate with high selectivity [5–12]. A review of the major previous works on the transformation of ethanol to valuable chemicals has been published elsewhere [9]. In brief, the authors summarized that supported noble metal catalysts are active in the production of acetic acid, whereas base metal oxides favor acetaldehyde. High selectivity toward ethyl acetate has been observed only over Cu/ZnO and Pd-based catalysts [6,9].

Nowadays, special attention is paid to the development of novel catalytic technologies for industrial production of acetaldehyde and acetic acid via one-step gas-phase conversion of ethanol. As shown by Raich and Foley [6], the gas-phase dehydrogenation of ethanol to acetaldehyde can be competed by a Wacker process based on the oxidation of ethylene. Using a palladium membrane reactor, they achieved a selectivity toward acetaldehyde of 70% at a conversion of ethanol of approximately 90%. Afterward it was found that oxide catalysts are more effective in these reactions. For instance, Li and Iglesia [7] have shown that multicomponent metal oxides Mo—V—Nb—O can catalyze the direct oxidation of ethanol to acetic acid with a selectivity of approximately 95% at 100% conversion. Mehlomakulu et al. [10] have found that ternary metal oxide catalysts $V_xMe_{1-x}SbO_4$ (Me = Fe, Al, Ga) are active in the gas-phase oxidation of ethanol to acetaldehyde with

* Corresponding author at: Boreskov Institute of Catalysis, Lavrentieva Ave. 5, 630090 Novosibirsk, Russia.
E-mail address: vvk@catalysis.ru (V.V. Kaichev).

http://dx.doi.org/10.1016/j.jcat.2016.02.022
0021-9517/

a selectivity of over 80%. The best catalytic performance was demonstrated by V_2O_5/TiO_2 nanoparticle catalysts that allowed producing acetaldehyde by the gas-phase oxidation of aqueous ethanol at approximately 180–185 °C with a selectivity higher than 90% at a conversion of ethanol above 95% [8]. Furthermore, a selectivity over 80% toward acetic acid could be achieved in this reaction at a low gas velocity at temperatures as low as 165 °C.

In this work we report the first results of our mechanistic study of the gas-phase selective oxidation of ethanol to acetaldehyde and acetic acid over titania-supported vanadium oxide catalysts. We used Fourier transform infrared spectroscopy (FTIR) and near-ambient pressure X-ray photoelectron spectroscopy, which allowed us to study the catalyst state and adsorbed species during the oxidation of alcohol [13,14]. The data are complemented by results of temperature-programmed reaction spectroscopy (TPRS) and kinetic measurements in a flow reactor.

2. Experimental

2.1. Catalyst preparation and characterization

All experiments were performed using a monolayer V_2O_5/TiO_2 catalyst, which was prepared as described in detail elsewhere [14,15]. In brief, a two-step procedure was used for synthesis of the catalyst. First, the TiO_2 support (anatase, 350 m^2/g) was impregnated with an aqueous solution of vanadyl oxalate via the incipient-wetness impregnation method and was subsequently dried at 110 °C for 12 h and then calcined in a flow of air at 400 °C for 4 h. According to chemical analysis, the catalyst consisted of 20 wt.% V_2O_5 and 80 wt.% TiO_2, and both polymeric surface vanadia species and supported V_2O_5 crystallites were detected by FTIR and X-ray diffraction (XRD) [14,15]. Second, to remove the V_2O_5 crystallites selectively, the catalyst was subsequently treated in a 10% aqueous solution of nitric acid at room temperature. After the washing process, the catalyst was calcined again in a flow of air at 400 °C for 4 h. This catalyst contained 12.5 wt.% V_2O_5, and no supported V_2O_5 crystallites were detected by XRD.

Earlier, it was found that vanadia might form different structures on titania surfaces, depending on the vanadia content and preparation techniques [16–22]. With the vanadia content under 10% of a monolayer, only isolated monomeric species with tetrahedral coordination exist under dehydrated conditions [17,20]. Polymeric structures such as chains and ribbons of VO_x units with octahedral coordination appear at a vanadia concentration above 20% of the monolayer [20]. The monolayer coverage of polymerized vanadia species on different oxides was measured by Raman spectroscopy and was found to be approximately 7–8 vanadium atoms/nm^2 for TiO_2 [18,19]. When the vanadium content exceeds what is necessary for the ideal monolayer, V_2O_5 crystallites are favorable. In our case the specific surface area of the washed catalyst was 115 m^2/g, which corresponded to the surface density of vanadia species of 7.3 V-atoms/nm^2. This means that polymeric vanadia species with a near-monolayer coverage exist mainly on the surface of the prepared catalyst. Such catalysts are usually referred to as monolayer catalysts [17].

2.2. Catalytic testing

The steady-state activity of the monolayer V_2O_5/TiO_2 catalyst was tested at atmospheric pressure in a differential reactor with a flow-circulating configuration [23]. The reactor was constructed from a Pyrex glass tube with a 12 mm inner diameter and a 50 mm length. A coaxial thermocouple pocket with a 4 mm outer diameter was fitted into the catalyst bed to control the temperature. The reactor was placed inside an electric oven. The temperature was controlled within ±0.5 °C by a K-type thermocouple. The feed consisted of ethanol, oxygen, and nitrogen in 1:4:15 M ratio. The concentrations of reactants and products were determined with an online gas chromatograph equipped with thermal conductivity and flame ionization detectors. Ethanol, acetaldehyde, acetic acid, diethyl ether, ethyl acetate, crotonaldehyde, ethylene, water, and CO_2 were analyzed with a Porapak T column, while CO, oxygen, and nitrogen were analyzed with an NaA molecular sieve column. All gas lines from the reactor to a sampling valve were maintained at 120 °C to prevent the condensation of reactants and products. Ethanol (A.C.S. reagent grade, 99% purity) obtained from Aldrich was used in all the experiments. The conversion of ethanol was calculated on the basis of measured inlet and outlet concentrations of ethanol. The selectivity toward each product was calculated as the amount of the detected product divided by the amount of converted ethanol using corresponding stoichiometric coefficients. The carbon balance was 97 ± 2%.

When the dependence of selectivity on the conversion was studied, changes in the conversion of ethanol were provided by varying the catalyst loading and the feed flow [14]. Under the conditions used, the conversion of ethanol increased nonlinearly with the contact time. The rate of consumption of ethanol is described well by the first-order equation with respect to ethanol concentration. According to this equation, the dependence of the conversion on the contact time is described by a curve increasing to a plateau.

2.3. XPS, TPRS, and FTIR measurements

The in situ XPS and TPRS experiments were performed at the ISISS (Innovative Station for In Situ Spectroscopy) beamline at the synchrotron radiation facility BESSY II (Berlin, Germany). The experimental station is described in detail elsewhere [13]. In brief, the station was equipped with a PHOIBOS-150 electron energy analyzer (SPECS Surface Nano Analysis GmbH), a gas cell, and a system of differential pumping, which allowed us to obtain high-quality core-level spectra at pressures up to 1 mbar. A powder sample was pressed into a thin self-supporting pellet. The pellet was mounted on a sapphire sample holder between two stainless steel plates. The first plate had a hole of 5 mm diameter for measuring the core-level spectra of the catalyst surface. The second plate was used for heating by a near infrared semiconductor laser (λ = 808 nm). The sample temperature was measured with a K-type thermocouple pressed directly against the rear of the sample. The flows of ethanol vapor and oxygen into the gas cell were regulated separately with calibrated mass-flow controllers (Bronkhorst High-Tech BV). The flow rate of ethanol in all the experiments was approximately 2 sccm. The total pressure in the gas cell was measured with an MKS Type 121A baratron (MKS Instruments Inc.) and was kept at a constant level during the experiments with the help of a special pumping system. This was 0.25 and 0.5 mbar in the experiments with ethanol and with an equimolar C_2H_5OH/O_2 mixture, respectively.

The synchrotron worked in the multibunch hybrid mode, which provided a constant photon flux. The C1*s*, Ti2$p_{3/2}$, V2$p_{3/2}$, and O1*s* core-level spectra were recorded at a photon energy of 720 eV. On the one hand, this provided acquisition of the core-level spectra at the same photon flux, which guaranteed the constant charge effect. On the other hand, the analysis depths for C, Ti, V, and O atoms were different; however, this was unimportant in this study. Charge correction was performed by setting the Ti2$p_{3/2}$ peak at 459.0 eV. The curve fitting was done with the CasaXPS software. The core-level spectra were resolved into their components after Shirley-type background subtraction. The lineshape of each component was considered to be a product of Lorentzian and Gaussian functions.

In the TPRS experiments the sample was heated at a constant rate from 50 to 350 °C in an equimolar mixture of ethanol and O_2. The heating rate was approximately 15 °C/min. The gas-phase composition was monitored continuously with a Prizma QMS-200 online quadrupole mass spectrometer (Pfeiffer Vacuum GmbH) connected through a leak valve to the gas cell. Before the experiments the mass spectrometer was calibrated with respect to ethanol, oxygen, and the reaction products CO, CO_2, H_2, H_2O, and CH_4. In the TPRS experiments, 11 MS signals with m/z ratios of 2 (H_2), 15 (CH_4), 18 (H_2O), 28 (CO), 29 (acetaldehyde), 32 (O_2), 42 (CH_2CO, ketene), 44 (CO_2), 46 (ethanol), 60 (acetic acid), and 88 (ethyl acetate) were monitored simultaneously.

To identify the reaction intermediates involved in the oxidation of ethanol, FTIR spectra were obtained in situ with a Cary 660 FTIR spectrometer (Agilent Technologies) within a temperature range of 100–300 °C using the same catalyst. The spectrometer was operated in the transmission mode using a specially designed quartz cell reactor with BaF_2 windows. The volume of the cell reactor was approximately 1.5 cm^3. The catalyst powder (35–50 mg) was pressed into a thin self-supporting pellet (15 mg/cm^2, 1 × 3 cm in size) and placed in the cell reactor. The FTIR experiments were performed at atmospheric pressure using a feed of 1.5 vol.% C_2H_5OH in air flowing at 50 sccm. Ethanol was dosed by bubbling air through a glass saturator filled with liquid ethanol at 0 °C. As a result, the molar ratio $C_2H_5OH:O_2:N_2$ was approximately 1:14:52. Before exposure to the reactant mixture, the sample was treated in a flow of air at 250 °C for 1 h. Subsequently, the cell reactor and the catalyst sample were cooled to the desired temperature, and the air flow was replaced with the ethanol/air mixture flow. The FTIR spectra were recorded in the range 1100–4000 cm^{-1} at a resolution of 4 cm^{-1} during stepwise heating at 100, 130, 150, 180, 200, 230, 250, and 300 °C.

The spectra of the gas phase were also recorded using a Cary 660 FTIR. In these experiments a special gas cell with optical path length approximately 70 mm was connected to the outlet of the cell reactor. Bands at 1065 cm^{-1} (Q branch of ν(C—O) band), 1760 cm^{-1} (P branch of ν(C═O) band), 1790 cm^{-1} (P branch of ν(C═O) band), 2115 cm^{-1} (R branch of ν(C═O) band), and 2360 cm^{-1} (P branch of ν(CO_2) band) were used for analysis of ethanol, acetaldehyde, acetic acid, CO, and CO_2, respectively.

3. Results and discussion

3.1. Catalytic results

The oxidation of ethanol was examined over the catalyst in the temperature range 110–230 °C. Acetaldehyde (CH_3CHO), acetic acid (CH_3COOH), diethyl ether ($(C_2H_5)_2O$), ethyl acetate (CH_3—COO—CH_2—CH_3), crotonaldehyde (CH_3CH═$CHCHO$), ethylene (C_2H_4), carbon oxides (CO and CO_2), and water were detected as products. The main results are shown in Fig. 1. One can see that the conversion of ethanol increases monotonically with the reaction temperature and attains 100% at 230 °C. At low temperatures, acetaldehyde is the major product. Its selectivity is 100% at 110 °C. The selectivity toward acetaldehyde decreases with temperature and the reaction shifts toward acetic acid. The formation of small amounts of ethyl acetate, ethylene, crotonaldehyde, CO, and CO_2 was also observed. Between 180 and 230 °C, acetic acid becomes the main reaction product. Its selectivity achieves approximately 60% at a conversion of ethanol near 95% at 200 °C. At temperatures above 250 °C, the oxidation of ethanol to CO and CO_2 predominates (not shown).

Fig. 1 also shows the temperature effect on the TOF (turnover frequency, rate per surface vanadium atom) of ethanol conversion over the monolayer V_2O_5/TiO_2 catalyst. This curve repeats the conversion graph: TOF monotonically increases with temperature and attains approximately 5×10^{-3} s^{-1} near 200 °C. The site time yield (STY), defined as the number of molecules of acetaldehyde or acetic acid formed per catalytic site and per unit time, was also calculated, using corresponding values of selectivity. It should be noted that the activity of the vanadia-based catalyst in the selective oxidation of ethanol is not high. For example, the TOF of the dehydrogenation of ethanol to acetaldehyde (without oxygen) over supported gold nanoparticles reaches 4–6 s^{-1} at 200 °C [9].

Fig. 2 demonstrates how the selectivity toward the main products depends on the conversion of ethanol at 130 and 180 °C. In both cases, at low conversion, the selectivity toward acetaldehyde is near 95%. However, at low temperature, only a small decrease of the selectivity toward acetaldehyde is observed (from 95% to 85%) when the conversion of ethanol increases from 20% to 90%. This is accompanied by the formation of crotonaldehyde, ethyl acetate, and carbon oxides (CO_x). The selectivity toward crotonaldehyde reaches 7–8%; the selectivity toward ethyl acetate and CO_x reaches only 4% and 2%, respectively. In contrast, at 180 °C the selectivity toward acetaldehyde is decreased significantly with increasing conversion of ethanol, which is accompanied with increasing selectivity toward acetic acid. The selectivity toward acetic acid reaches 46% at 80% conversion of ethanol. A notable yield of carbon oxides is also observed at a conversion of ethanol near 90%. Such dependence of selectivity on the reaction temperature (Fig. 1) and on the conversion of ethanol (Fig. 2) suggests a consecutive scheme for the formation of the reaction products in the entire temperature range: ethanol → acetaldehyde → acetic acid → CO_x.

3.2. In situ FTIR

The formation of adsorbed species during the oxidation of ethanol was examined by infrared spectroscopy. Fig. 3 displays the FTIR spectra obtained in situ in the temperature range 100–250 °C. In this experiment a mixture of 1.5 vol.% C_2H_5OH in air was passed through the IR cell reactor loaded with the monolayer V_2O_5/TiO_2 catalyst. The spectrum of the catalyst before exposure to the reactant mixture and the spectrum of gas-phase ethanol were subtracted from the raw FTIR spectra to identify the contributions of the adsorbed species. In the spectrum acquired at 100 °C, positive bands appear at 2977, 2934, 2877, 1730, 1664, 1532, 1444, 1383, 1232, 1144, 1090, and 1040 cm^{-1}. According to the literature [24–28], most of these features can be assigned to the vibration modes of molecularly adsorbed ethanol (CH_3CH_2OH) and ethoxide (CH_3—CH_2O^-) species, as outlined in Table 1. Both species are characterized by similar bands of C—H stretching vibrations at 2977, 2934, and 2877 cm^{-1} and C—O stretching vibrations at 1144, 1090, and 1040 cm^{-1}, as well as CH_3 bending vibrations at 1444 and 1383 cm^{-1}. The extra peak at 1232 cm^{-1} is certainly due to δ (OH) mode of molecularly adsorbed ethanol. This band disappears completely at 130 °C, indicating dissociation or desorption of ethanol. In contrast, the bands at 2977, 2934, 2877, 1144, 1090, and 1040 cm^{-1} disappear only at 200 °C. The presence of two bands at 1090 and 1040 cm^{-1} indicates that at least two kinds of adsorbed ethoxide species are formed. The bands at 1144 and 1090 cm^{-1} may be characterized as monodentate ethoxide, while the band at 1040 cm^{-1} is assigned to two bridging ethoxides [26]. The negative signal in the hydroxyl region near 3650 cm^{-1} is due to removing OH groups. This process also stops at temperature above 200 °C.

It is important to note that the formation of the ethoxide species is accompanied by a decrease in intensity of the band assigned to the first overtone of ν(V═O) at 2029 cm^{-1}. The corresponding negative band is presented in the inset in Fig. 3. This means that the terminal vanadyl groups are involved in the oxidation of

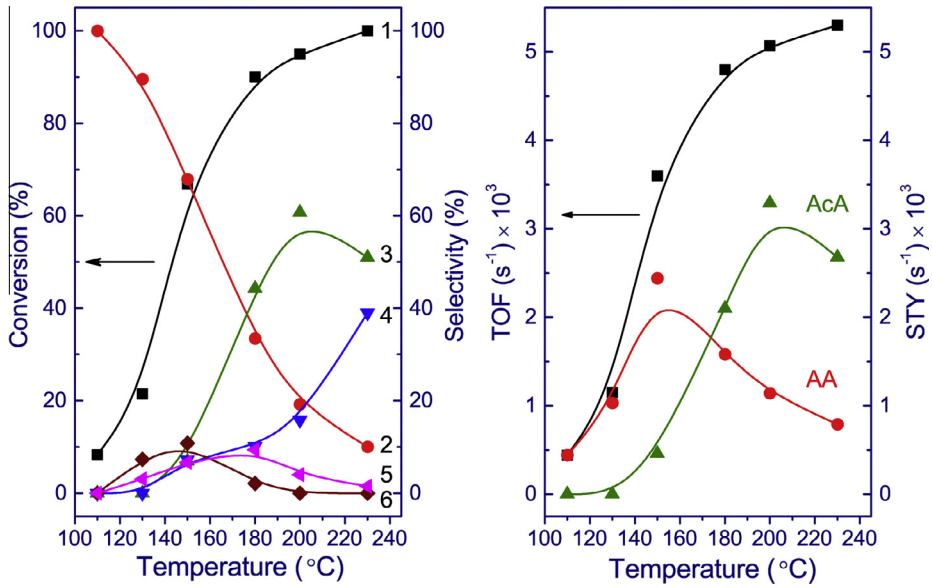

Fig. 1. Ethanol conversion (1) and selectivity toward acetaldehyde (2), acetic acid (3), carbon oxides (4), ethyl acetate (5), and crotonaldehyde (6) vs. temperature observed over the monolayer V_2O_5/TiO_2 catalyst (left panel). Ethylene was detected between 130 and 180 °C with selectivity not exceeding 0.1%; diethyl ether was detected between 150 and 180 °C with selectivity of 0.4–0.5%. Turnover frequency (TOF) for ethanol conversion and site time yield (STY) of acetaldehyde or acetic acid as a function of the reaction temperature (right panel).

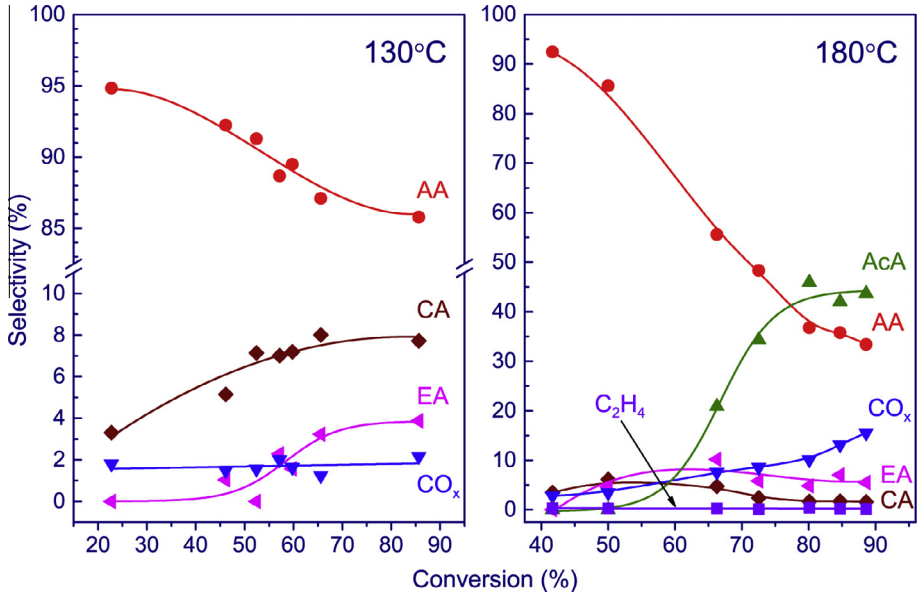

Fig. 2. Selectivity toward acetaldehyde (AA), acetic acid (AcA), carbon oxides (CO_x), ethyl acetate (EA), crotonaldehyde (CA), and ethylene vs. conversion measured at 130 and 180 °C. Changes in the conversion of ethanol were provided by varying the catalyst loading and the feed flow [14].

ethanol. This process is accompanied by formation of hydrogen bonds, which is reflected in a broad band observed at 3400 cm^{-1}.

Not all of the features observed in the spectrum acquired at 100 °C can be assigned to molecularly adsorbed ethanol and ethoxide species. Taking into account the catalytic data (Fig. 1), we can speculate that the main products of the oxidation of ethanol, such as acetaldehyde and acetic acid, can also be adsorbed onto the catalyst's surface, at least at low temperatures. From this point of view, we attribute the strong bands at 1730 and 1680 cm^{-1} to adsorbed acetaldehyde. Indeed, acetaldehyde adsorbed on TiO_2 is characterized by the ν(C═O) vibrations at 1715–1723 cm^{-1} [24,25]. Both these bands decrease in intensity with rising temperature. Other bands developed by heating the catalyst can be attributed to adsorbed acetate complex and acetic acid. According to the previous results taken from the literature [24–26,29], the bands at 1532 and 1444 cm^{-1} could be assigned to the ν_{as}(COO) and ν_s(COO) modes, respectively, of adsorbed acetate complexes. The bands of acetate species progressively increase in intensity with heating up to around 200 °C but decrease precipitously between 200 and 250 °C. Acetic acid is represented by the band near 1664 cm^{-1} due to the carbonyl stretching mode [25,29]. This band appears in the spectra acquired at 100 and 130 °C, and its intensity decreases with temperature. Finally, at 300 °C no bands are observed in the spectrum. It should be noted that the bands assigned to acetate species start shifting and broadening progressively at 200 °C. We tentatively associate this effect with the formation of carbonate species that occurs at high temperatures. Usually, coordinated carbonates are characterized by two bands

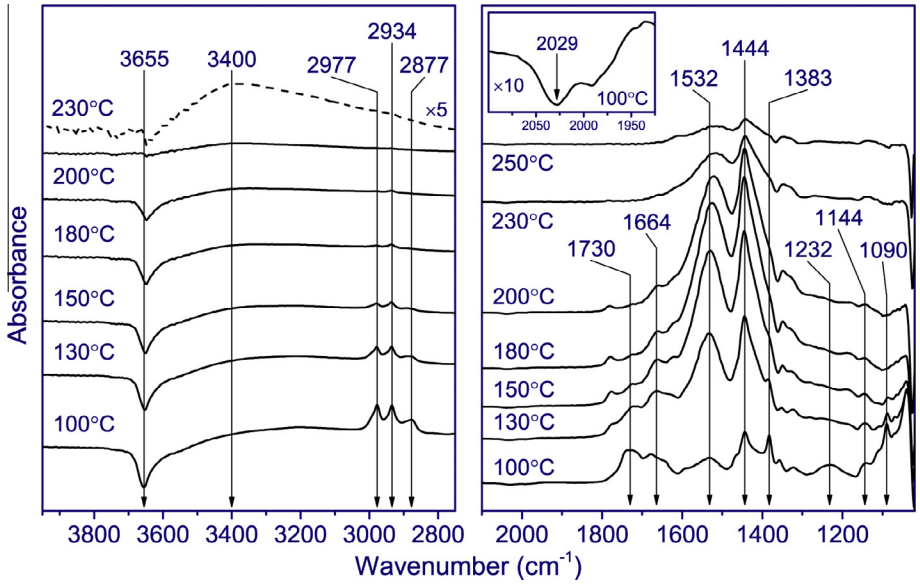

Fig. 3. FTIR spectra obtained in situ during the oxidation of ethanol over the monolayer V_2O_5/TiO_2 catalyst at 100, 130, 150, 180, 200, 230, and 250 °C. Part of the spectrum in the vanadyl-groups region obtained at 100 °C is present in the inset.

Table 1
Vibrational mode assignments for surface species following oxidation of ethanol.

Mode	Surface species	Wavenumber (cm^{-1})			
		TiO_2 [24]	TiO_2 [25]	CeO_2 [26]	Al_2O_3 [27]
$\nu_{as}(CH_3)$	Ethanol	2971	2971	2965	2970
$\nu_{as}(CH_2)$	Ethoxide	2931	2931	2925	2930
$\nu_s(CH_3)$	Ethoxide	2868	2872, 2869	2864	2900
ν(C═O)	CH_3CHO_{ads}	1715	1718–1723	–	–
ν(C═O)	CH_3COOH_{ads}	–	1684	–	–
ν_{as}(COO)	Acetate	1540, 1583	1542, 1537	1584	–
$\delta(CH_2)$ scissoring	Ethoxide	1474	–	–	–
$\delta_{as}(CH_3)/\delta_s(CH_3)$	Acetate	–	1469/1340	–	1450/1390
$\delta_{as}(CH_3)/\delta_s(CH_3)$	Ethoxide	1451/1380	1450/1380	1475/1365	–
ν_s(COO)	Acetate	1437, 1415	1446, 1443, 1438, 1421	1443	–
CH_2 wagging	Ethoxide	1356	1356	–	–
δ(OH)	Ethanol	1274	1274	1260	–
ν(C—O) monodentate	Ethoxide	1147, 1111	1147, 1113	1120, 1096	1115
ν(C—C)	Ethanol	1100	–	–	–
ν(C—O) bidentate	Ethoxide	–	1052	1050	1070
ν(C—C)	Ethoxide	1074	–	–	–

in the range between 1400 and 1600 cm^{-1} due to the asymmetrical stretching mode.

We also studied the interaction of ethanol with the V_2O_5/TiO_2 catalyst in the absence of O_2 in the gas phase. Fig. 4 demonstrates the spectra acquired in situ in the temperature range 100–250 °C. The spectrum obtained at 100 °C is similar to the spectra acquired at the same temperature in the presence of O_2 (see Fig. 3). The only difference is associated with the appearance of a rather narrow band with a maximum at approximately 1645 cm^{-1}. This band could be assigned to the ν(C═C) stretching mode of adsorbed crotonaldehyde [30]. The position of the ν(C═O) band in the infrared spectrum of this complex is very close to the band position of adsorbed acetaldehyde [29]. Crotonaldehyde is a product of acetaldehyde condensation. Acetate complexes are the main surface species formed during the interaction of ethanol with the catalyst at 130–250 °C. The surface concentration of acetates is much higher in the absence of O_2 than in the presence of O_2 in the gas phase (Fig. 5). It is important that adsorbed acetic acid is not observed in the absence of O_2 (see absorbance near 1664 cm^{-1} due to the carbonyl stretching mode of adsorbed acetic acid [25,29]). Carbonate complexes appear at 250 °C. A strong band at 1780 cm^{-1} and a weak band at 1850 cm^{-1} are observed additionally in the spectra obtained at temperatures between 130 and 250 °C. We assume that these bands could be assigned to asymmetric and symmetric ν(C═O) modes of adsorbed maleic anhydride, which is a product of the oxidation of crotonaldehyde [30]. Unfortunately, because we used a gas cell with a small volume and a rather short optical path, we could not observe the bands of maleic anhydride in the gas phase.

In additional experiments, the gas-phase composition in the outlet of the cell reactor with the V_2O_5/TiO_2 catalyst loaded was analyzed by FTIR. The intensity of the IR bands due to ethanol, acetaldehyde, acetic acid, CO, and CO_2 measured during the stepwise heating of the catalyst in the ethanol/air mixture is shown in Fig. 6a. One can see that the intensity of the ethanol signal decreases strongly after heating above 100 °C, indicating that the oxidation of ethanol occurs under these conditions. In full agreement with the results of catalytic tests (Fig. 1), the acetaldehyde signal is undetected below 90 °C, and then its intensity increases strongly, reaching a maximum at 150 °C. At higher temperature the signals of acetic acid, CO, and CO_2 are observed. The yield of acetic acid achieves a maximum near 200 °C, while the yield of

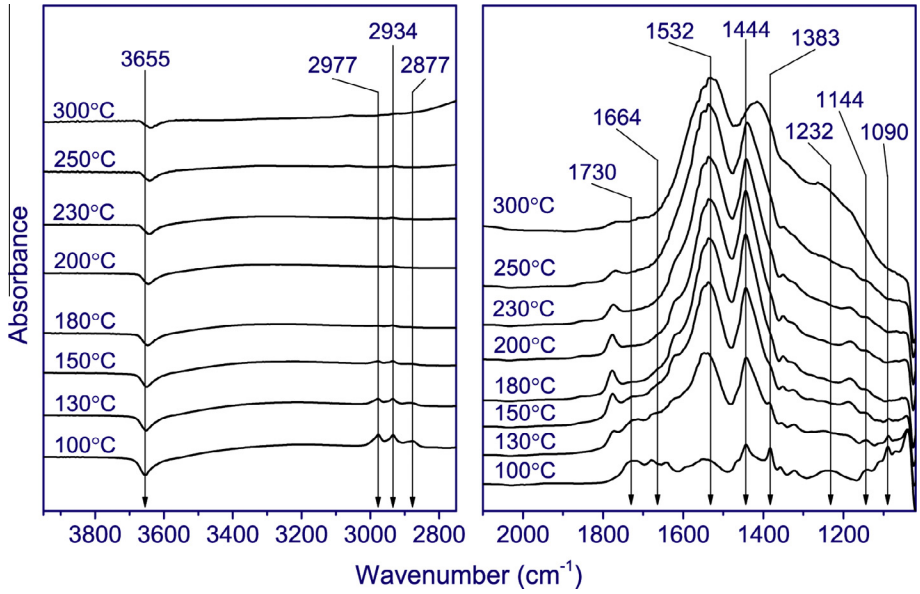

Fig. 4. FTIR spectra of the monolayer V_2O_5/TiO_2 catalyst obtained in situ under flows of ethanol/helium mixture at 100, 130, 150, 180, 200, 230, 250, and 300 °C.

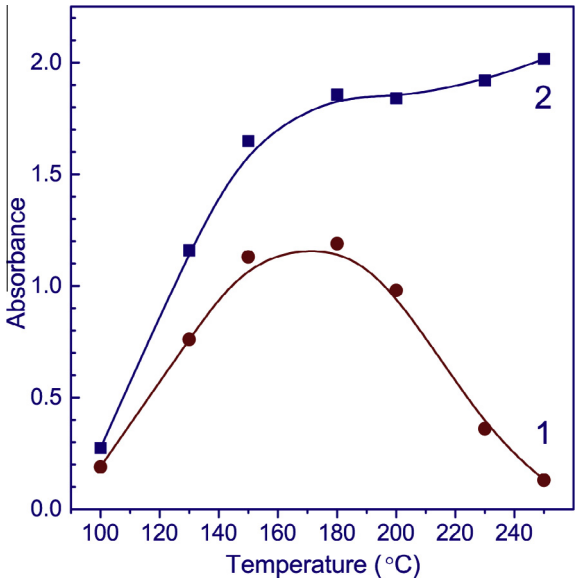

Fig. 5. The dependence of the intensity of the $\nu_{as}(COO)$ band on temperature obtained in the presence (1) and in the absence (2) of O_2 in the gas phase.

CO and CO_2 increases with the reaction temperature. In the absence of O_2 in the gas phase, the only detectable gaseous product of the transformation of ethanol is acetaldehyde (see Fig. 6b). Acetaldehyde appears at 90 °C, and its concentration increases with the temperature. It should be emphasized that acetic acid and carbon oxides do not form at temperatures between 100 and 250 °C in the absence of O_2.

3.3. In situ XPS and TPRS

The XPS spectra were measured during the heating of the monolayer V_2O_5/TiO_2 catalyst in a stepwise manner in ethanol and in an equimolar C_2H_5OH/O_2 mixture. The corresponding V2$p_{3/2}$ and Ti2$p_{3/2}$ core-level spectra are presented in Figs. 7 and 8. In both cases, before exposure to the reactant mixture or ethanol, the catalyst was pretreated in 0.25 mbar of flowing O_2 at 350 °C for 30 min directly inside the XPS reaction gas cell. This treatment led to full oxidation of vanadium, and as a result, only a narrow single peak at 517.7 eV corresponding to the V^{5+} state was observed in the V2$p_{3/2}$ spectra. According to the literature data [14,31–36], bulk and supported V_2O_5 are characterized by V2$p_{3/2}$ binding energy in the range 517.0–517.7 eV, whereas the V2$p_{3/2}$ binding energy of V_2O_4 and V_2O_3 is within the ranges 516.0–516.5 and 515.8–515.9 eV, respectively.

The vanadium cations underwent complete reduction from V^{5+} to V^{4+} and V^{3+} by ethanol even at 110 °C. This conclusion arose from analysis of the V2$p_{3/2}$ spectra presented in Fig. 7a. In the ethanol flow, the typical V2$p_{3/2}$ spectrum of the fully oxidized catalyst exhibiting a single peak transformed into the spectrum with two peaks at 516.5–516.6 and 515.4–515.5 eV, which can be attributed to V^{4+} and V^{3+}, respectively. The fraction of the V^{3+} state grows slightly with temperature. The results of curve-fitting analysis are presented in Table 2. The following treatment in oxygen at 350 °C led again to the full oxidation of vanadium to V^{5+}. These data indicate that supported vanadium could undergo reversible oxidation and reduction during the oxidation of ethanol.

In contrast, no changes were detected in the Ti2$p_{3/2}$ spectra over the entire temperature range: the spectra consist of only a narrow peak at 459.0 eV with a full width at half maximum (FWHM) of approximately 1.1 eV (Fig. 7b), which is typical of bulk TiO_2 [14]. This means that titanium in the catalyst support remains in the Ti^{4+} state under reaction conditions. This is an interesting and rather unexpected result. Indeed, in the chemically similar V_2O_5/CeO_2 catalysts, the Ce^{4+} cations become reduced in the selective oxidation of ethanol. Also, some authors suppose that Ti^{4+} cations in the V_2O_5/TiO_2 catalysts also undergo partial reduction during this reaction (see Ref. [47] and references therein).

Fig. 8a displays the V2$p_{3/2}$ spectra obtained in situ during the oxidation of ethanol in the temperature range 110–230 °C. All the V2$p_{3/2}$ spectra consist of two peaks at 517.6–517.7 and 516.4–516.5 eV that can be attributed to V^{5+} and V^{4+}, respectively. An exception is the spectrum obtained at 50 °C (spectrum not shown), where an additional weak peak due to V^{3+} is observed at 515.7 eV. These data indicate that in the presence of O_2 the fast reoxidation of V^{3+} and V^{4+} to V^{5+} occurs. Again, the Ti2$p_{3/2}$ spectra consist of a single sharp peak at 459.0 eV, which corresponds only to Ti^{4+} (Fig. 8b).

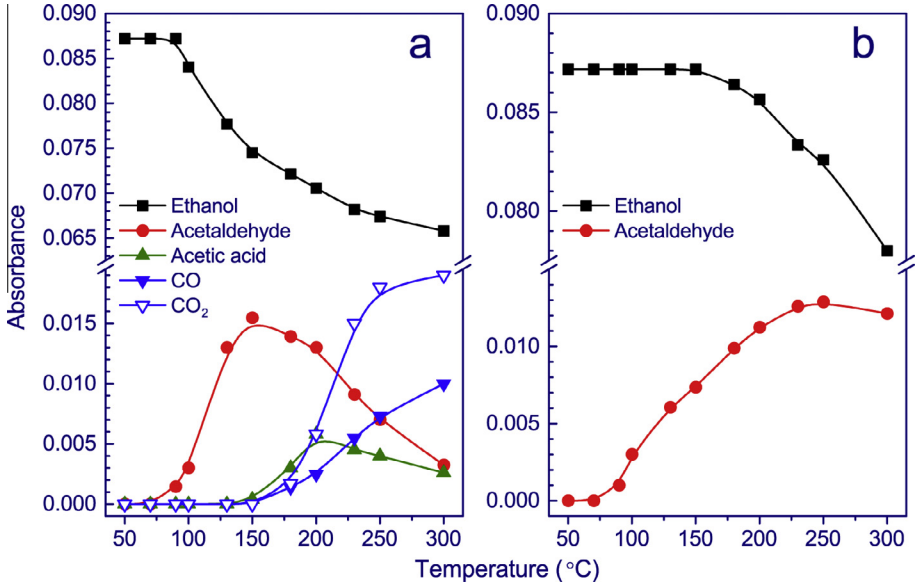

Fig. 6. Infrared-absorption intensities of ethanol and main detected products (acetaldehyde, acetic acid, CO, and CO_2) measured during ethanol oxidation over the monolayer V_2O_5/TiO_2 catalyst as a function of temperature (a) and infrared-absorption intensities of ethanol and acetaldehyde formed from ethanol over the monolayer V_2O_5/TiO_2 catalyst without O_2 in the gas phase as a function of temperature (b).

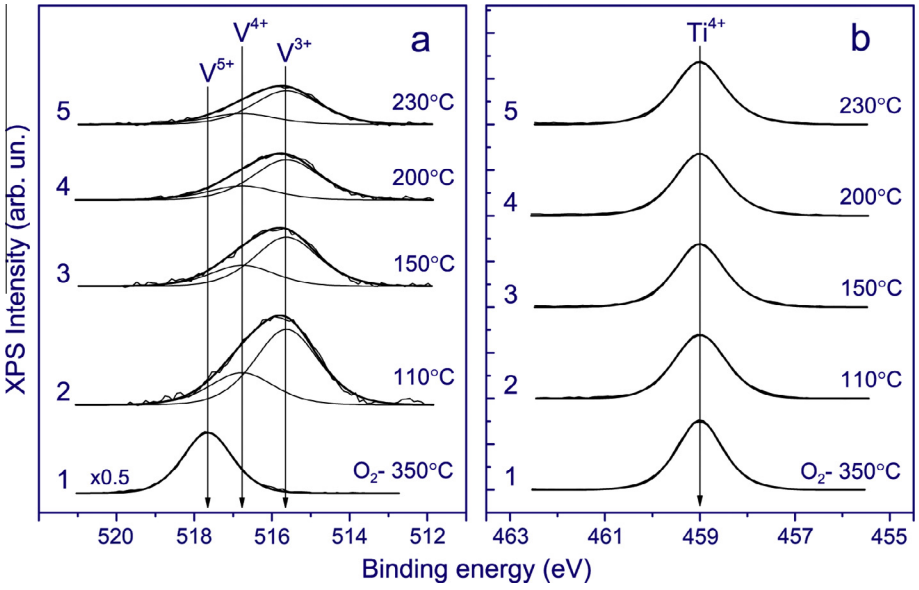

Fig. 7. Normalized V2$p_{3/2}$ (a) and Ti2$p_{3/2}$ (b) core-level spectra of the monolayer V_2O_5/TiO_2 catalyst. Spectra 1 were obtained in 0.25 mbar flowing O_2 at 350 °C; spectra 2–5 in 0.25 mbar flowing ethanol at 110, 150, 200, and 230 °C, respectively.

The C1*s* core-level spectra obtained in situ during the heating of the monolayer V_2O_5/TiO_2 catalyst in a stepwise manner in both ethanol and the C_2H_5OH/O_2 mixture are presented in Fig. 9. The spectra obtained in ethanol are described well by four peaks at 284.5, 285.15, 286.4, and 289.1 eV (Fig. 9a). Two strong peaks at 285.15 and 286.4 eV, which dominate at low temperatures, could be assigned to two chemically distinct carbon atoms of molecularly adsorbed ethanol and surface ethoxide species. The different local environments of these two carbons induce a chemical shift in the C1*s* binding energy. The first peak corresponds to carbon atoms in the methyl groups, while the second peak corresponds to carbon atoms bonded with oxygen. Indeed, ethanol adsorbed molecularly on a Pd(1 1 0) single crystal is characterized by a C1*s* spectrum consisting of two peaks at 285.0 and 286.0 eV [37]. For ethanol adsorbed molecularly on TiO_2, two peaks at 285.3 and 286.6 eV are also observed [38]. The surface ethoxide species on TiO_2 is characterized by C1*s* peaks at 285.5 and 286.8 eV as well [39]. Another peak at 289.1 eV could be assigned to surface acetate, which is characterized on TiO_2, for example, by a C1*s* peak near 290 eV [39]. The C1 s peak at 284.5 eV could be assigned to different adsorbed CH_x species ($x = 0–3$) produced by C—C bond scission and further dehydrogenation [40–42]. The decrease of the C1*s* peaks at 285.15 and 286.4 eV with the reaction temperature could be attributed to desorption of ethanol. The increase of the C1*s* peak at 284.5 eV is due to the accumulation of different CH_x species on the catalyst surface. The decrease of the C1*s* peak of acetate is most likely due to its decomposition at higher temperatures.

The C1*s* spectra obtained in the C_2H_5OH/O_2 mixture (Fig. 9b) consist of the same four peaks at 284.5, 285.15, 286.4, and 289.1 eV and an extra peak at 286.1 eV. In agreement with the FTIR

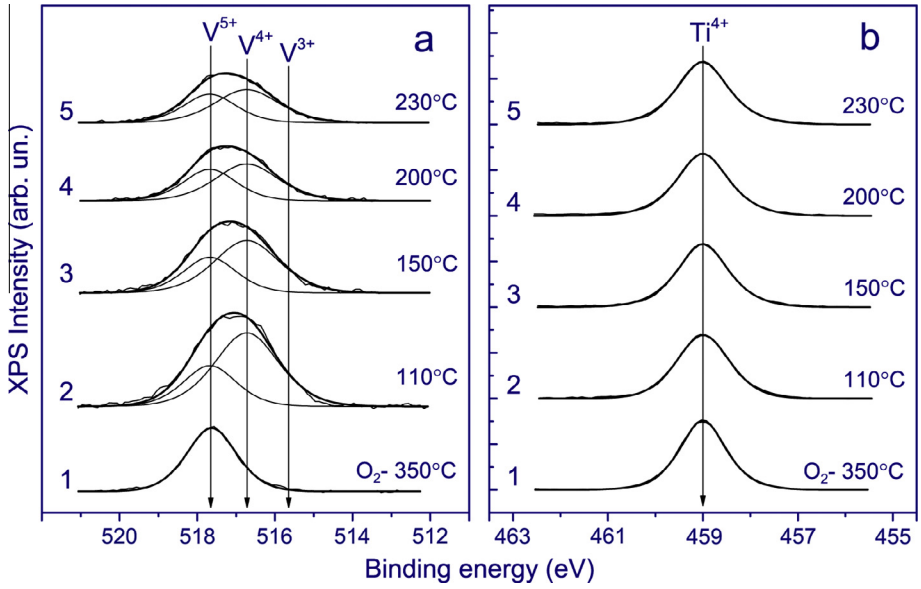

Fig. 8. Normalized V2$p_{3/2}$ (a) and Ti2$p_{3/2}$ (b) core-level spectra of the monolayer V_2O_5/TiO_2 catalyst. Spectra 1 were obtained in 0.25 mbar flowing O_2 at 350 °C; spectra 2–5 under a flow of the equimolar C_2H_5OH/O_2 mixture at 0.5 mbar during stepwise heating at 110, 150, 200, and 230 °C.

Table 2
The V2$p_{3/2}$ binding energies and FWHM of the Ti2$p_{3/2}$ peaks shown in Figs. 7 and 8 (the relative intensities of the different components (%) are presented in parentheses).

Gas phase composition	*T*, °C	FWHM of Ti2$p_{3/2}$ peak, eV	V2$p_{3/2}$, eV (%)		
			V^{5+}	V^{4+}	V^{3+}
O_2	300	1.12	517.66 (100)	–	–
$CH_3OH + O_2$	100	1.05	517.73 (51)	516.50 (49)	–
$CH_3OH + O_2$	150	1.07	517.68 (59)	516.43 (41)	–
$CH_3OH + O_2$	200	1.09	517.63 (67)	516.40 (33)	–
CH_3OH	50	1.10	–	516.60 (41)	515.54 (59)
CH_3OH	100	1.12	–	516.60 (31)	515.42 (69)
CH_3OH	150	1.13	–	516.60 (28)	515.45 (72)
CH_3OH	200	1.14	–	516.50 (32)	515.47 (68)

data (Fig. 3), the acetate C1*s* peak at 289.1 eV is observed only at high temperatures within the range 150–250 °C. The origin of the peaks at 284.5 and 286.1 eV is not evident. Taking into account the FTIR data, we can speculate that this doublet originates from molecularly adsorbed ethanol. The shift of the C1*s* peaks to lower binding energy in comparison with the peaks observed under a flow of ethanol may be determined by the different oxidation state of vanadium on the catalyst surface. In ethanol vanadium is fully reduced and V^{3+} and V^{4+} cations are on the surface, while in the C_2H_5OH/O_2 mixture vanadium is partially reduced and V^{4+} and V^{5+} cations are mainly on the surface. The peaks at 285.15 and 286.4 eV observed at low temperatures could be assigned to the ethoxide species adsorbed onto the partially reduced vanadia surface. The peaks decrease in intensity with the temperature rise, also in good agreement with the FTIR data.

It should be noted that due to physical limits the in situ XPS technique could be used under mbar pressures only [13]. Comparison of the XPS data with the results of FTIR and kinetics measurements performed in a flow reactor at atmospheric pressure is only possible if there is no "pressure gap". The TPRS technique was applied to verify this statement. The monolayer V_2O_5/TiO_2 catalyst was heated inside the in situ XPS reaction gas cell in the CH_3OH/O_2 mixture; the product distribution was monitored with a differentially pumped mass spectrometer. The catalyst was pretreated in 0.25 mbar of flowing O_2 at 350 °C for 30 min.

Fig. 10 displays the TPRS data obtained in the temperature range 75–320 °C. In good agreement with the results of kinetics measurements (Fig. 1), the reaction starts near 130 °C. However, within the entire temperature range, the main products are acetaldehyde and water. No acetic acid was detected by mass spectrometry in this experiment. The formation of CO occurs at temperatures above approximately 200 °C. The yield of CO_2 is negligible. Taking into account the FTIR data (Fig. 6b), we can speculate that the difference between the TPRS and kinetics measurements could be determined by the difference in the partial pressure of oxygen and ethanol. At low pressure the oxidation of ethanol to acetaldehyde proceeds at a high rate over the V_2O_5/TiO_2 catalyst; however, the balance between production of acetaldehyde and acetic acid is shifted because of desorption of acetaldehyde from the catalyst surface. As a result, under these conditions, the yield of CO exceeds the yield of CO_2, while in the FTIR experiments the reverse dependence was observed (Fig. 6a). Indeed, CO is a product of the decomposition of ethanol, which is more likely to occur via breaking C—C bonds in adsorbed CH_3—CH_x—O species and subsequent dehydrogenation of CH_xO to CO [40–42]. This process is accompanied by the appearance of the C1*s* peak at 284.5 eV corresponding to the adsorbed CH_x species (Fig. 9). The CO_2 is more likely to form via decomposition of carbonate species, which in turn are produced from acetate species. Correspondingly, the low yield of CO_2 correlates with the low yield of acetic acid (Fig. 10). Hence, we believe that the catalytic behavior under mbar pressure follows the same trends as observed under atmospheric pressure, and the results of the in situ XPS study are therefore fully applicable.

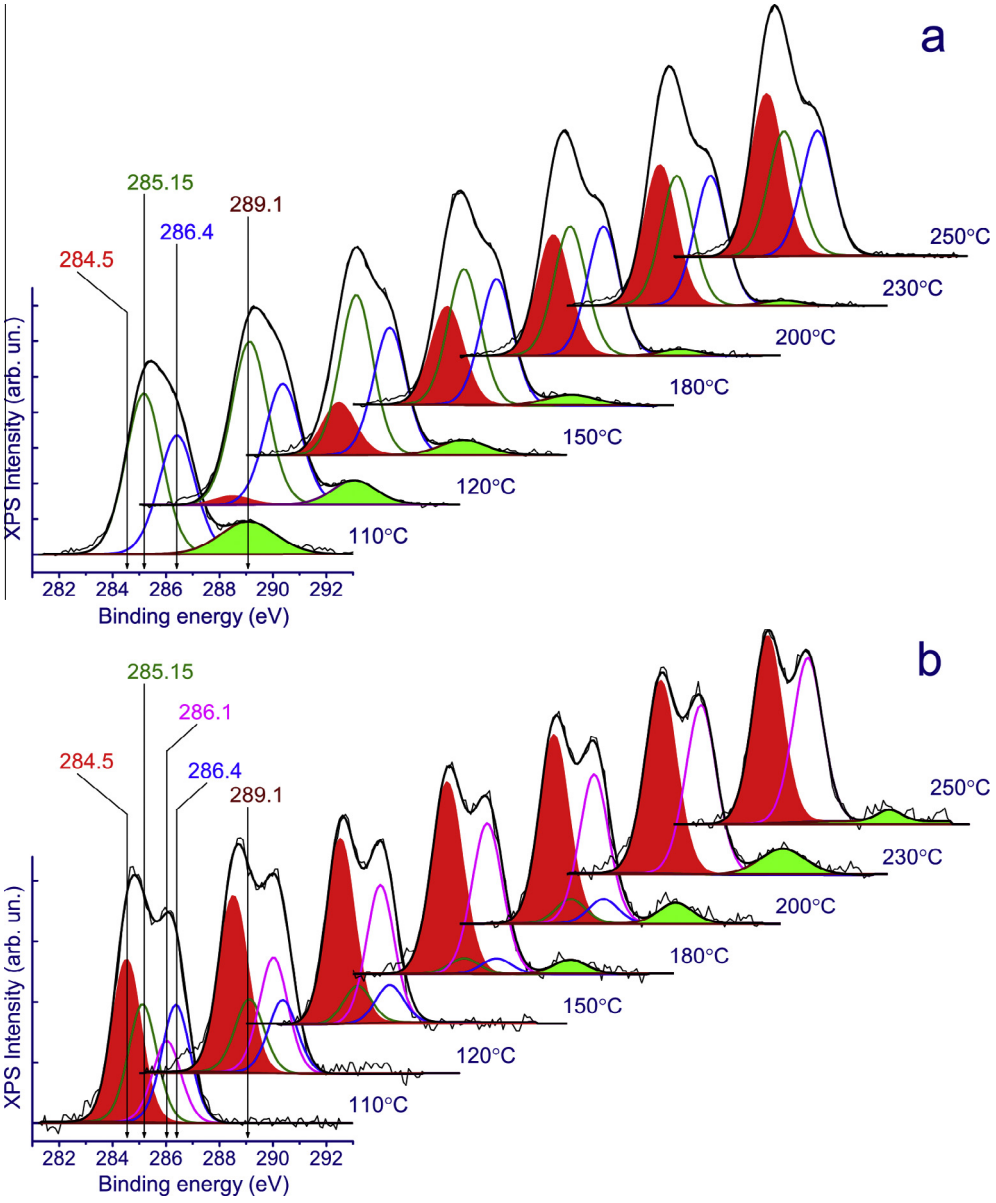

Fig. 9. Normalized C1*s* core-level spectra acquired simultaneously with the V2$p_{3/2}$ and Ti2$p_{3/2}$ spectra presented in Figs. 7 and 8 during heating of the monolayer V_2O_5/TiO_2 catalyst in the stepwise manner in ethanol (a) and in the equimolar C_2H_5OH/O_2 mixture (b). The spectra are normalized by integral intensity of the Ti2*p* spectra.

4. Discussion

The presented data allow us to describe in detail the mechanism for the oxidation of ethanol over vanadia–titania catalysts, including the structure and consecutive transformations of the surface complexes of ethanol, the forms of reactive oxygen species, and redox transformations of the active centers. The mechanism can be described in terms of the sequence of elementary steps depicted in Fig. 11. Note that this mechanism agrees well with the microkinetic scheme proposed by Li and Iglesia [7] for the oxidation of ethanol over multicomponent metal oxide catalysts. Using mathematical modeling, they have determined the main reaction steps and reaction constants that described the Mars–van Krevelen redox cycle for the oxidation of ethanol to acetaldehyde and acetic acid. However, only complementary in situ XPS and FTIR data made it possible to link the redox processes to the formation of different intermediates.

Our mechanism resembles the one previously proposed for methanol oxidation over vanadia–titania catalysts, which explains the formation of dimethoxymethane, formaldehyde, methyl formate, and formic acid [14,43]. However, some details are rather different. In both cases, the catalytic cycle begins with the catalyst in the oxidized state. DFT calculations for the oxidation of methanol [44,45] have shown that at the first step the alcohol adsorbs dissociatively, resulting in cleavage of a V—O—Ti bond to form V—OCH_3 and Ti—OH species. According to the previous experimental study [46], the terminal vanadyl groups are not involved in the oxidation of methanol. Ethanol also adsorbs intact on the acid–base sites of the catalyst and further can dissociate to form the adsorbed ethoxide species and OH group. Because the formation of the ethoxide species is accompanied by a decrease in the bands due to ν(V=O) and a strong band is observed in the IR spectra due to H-bonded hydroxyl groups (Fig. 3), we believe that the chemisorption of ethanol is a heterolytic process, during which the proton from the alcohol hydroxyl group is transferred to the vanadyl oxygen atom and the oxidation state of vanadium changes from V^{5+} to V^{4+} (Step 1). It should be noted that Beck et al. [47] have another point of view suggesting that the hydroxyl group

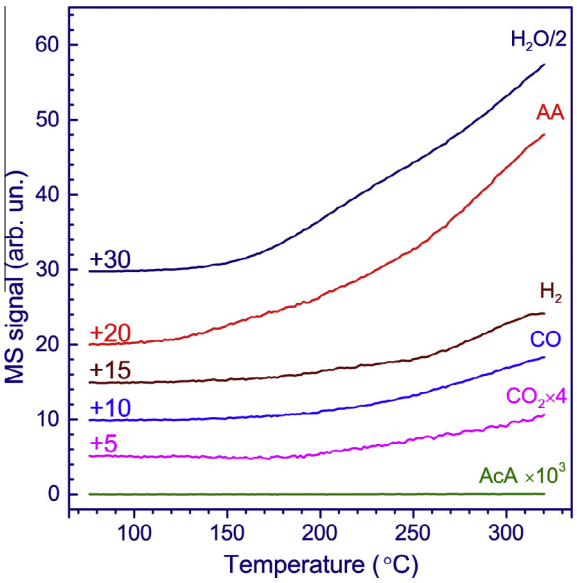

Fig. 10. TPRS data obtained during heating OF the monolayer V_2O_5/TiO_2 catalyst under 0.5 mbar of flowing equimolar C_2H_5OH/O_2 mixture.

bonds with cations of the support. However, this model contradicts our FTIR data, because in this case the formation of hydrogen bonds is limited.

Acetaldehyde is formed in a subsequent step via a transfer of a proton from the CH_2 group to the catalyst, which is accompanied by the partial reduction of the next vanadium atom (Step 2). According to deuterium isotopic substitution experiments [48,49], α-C—H bond breaking is a rate-determining step in the oxidation of ethanol to acetaldehyde. We believe that during this process the effect of the support must be significant, and by analogy with the oxidation of methanol [43], the nascent hydroxyl group may be bonded with the titanium cations. The OH group ultimately recombines with another OH to form H_2O and the vanadyl oxygen species (Step 3); adsorbed acetaldehyde can desorb as a product. Hence, the terminal V=O bond and the bridge V—O—Ti bond are involved in the oxidative dehydrogenation of ethanol through the transfer of two electrons. This conclusion is confirmed by the in situ data obtained during the oxidation of ethanol at low temperatures: the adsorbed ethanol and acetaldehyde species were detected by FTIR (Fig. 3) and the partial reduction of V^{5+} to V^{4+} was detected by XPS (Fig. 8). Moreover, the reduction of V^{5+} cations in such processes was predicted by Döbler et al. [50], who studied the oxidation of methanol to formaldehyde on silica-supported vanadium oxide using DFT. Unfortunately, they used the simplest model of active sites consisting of isolated vanadium cations. As a result, during formaldehyde formation the oxidation state of vanadium changed from V^{5+} to V^{3+}.

It should be stressed that the exact role of the bridge V—O—Ti bond in the oxidative dehydrogenation of ethanol to acetaldehyde is still a topic of debate. For example, Kilos et al. [48], based on kinetics measurements, have developed a mechanism for the oxidation of ethanol to acetaldehyde over VO_x/Al_2O_3 catalysts in which only the terminal V=O bond and the bridge V—O—V bond are involved.

Since the selectivity toward acetic acid increases with the ethanol conversion (Fig. 2), we can speculate that the formation of acetic acid should occur as a consecutive reaction by the oxidation of initially formed acetaldehyde. We believe that adsorbed acetaldehyde reacts with lattice oxygen atoms to form the adsorbed acetate species (Step 4), which are detected by FTIR during the oxidation of ethanol (Fig. 3). The formation of acetate species from acetaldehyde has been observed on Fe_2O_3 and vanadia–titania catalysts as well [29,51]. The formation of acetate is accompanied by the further reduction of vanadium to V^{3+} and the formation of oxygen vacancy. It is confirmed by the XPS data (Fig. 7), which indicate the high concentration of the adsorbed acetate species and the V^{3+} cations observed in ethanol at 110 °C. It is very important that we did not observe any acetic acid and CO_2 among products in the absence of O_2 in the gas phase (Fig. 6b). This means that the formation and desorption of acetic acid, as well as CO_2, do not occur on the reduced catalyst, due to the high stability of the acetate species. At least partial oxidation of the catalyst is needed for acetic acid formation. It is more probable that this effect is due to a high activation barrier for the formation of acetic acid from the surface acetate species over reduced vanadia.

Therefore, after the transformation of acetaldehyde to acetate species adsorbed onto the V^{3+} active sites, the partial or full oxidation of the vanadium cations by gas-phase oxygen takes place. Unfortunately, we have not found any information about this step in the literature, and it is not clear how this process is realized. We assume that the full oxidation of vanadium takes place accompanied by the formation of adsorbed acetic acid on the V^{5+} cation (Step 5). This is in good agreement with the results by Avdeev and Parmon [52], who used DFT calculations to show that the heat of desorption of formic acid from reduced vanadium sites was

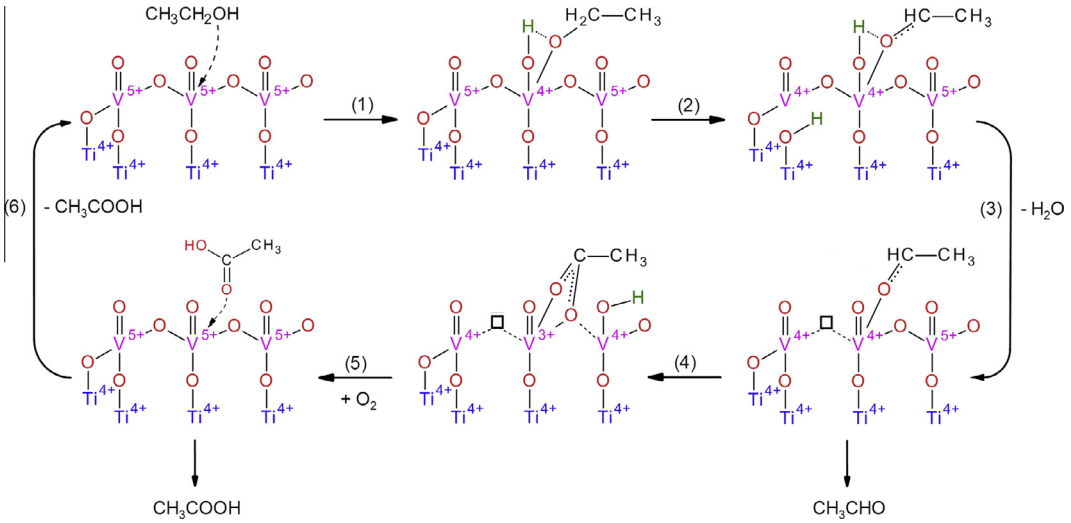

Fig. 11. Reaction scheme for the selective oxidation of ethanol over the monolayer vanadia–titania catalyst.

about 33 kcal/mol, whereas the heat of formic acid desorption from oxidized vanadia sites was equal to 16 kcal/mol. Thus, the catalyst reoxidation results in a weakening of the carboxylate–vanadium bond and desorption of acetic acid that finally locks the catalytic cycle (Step 6). Alternatively, the last process may be separated into two steps: the partial oxidation of V^{3+} to V^{4+}, accompanied with weakening of the carboxylate–vanadium bond and following desorption of acetic acid. In this case the catalytic cycle is finally closed by oxidizing the V^{4+} cations via irreversible chemisorption of oxygen to form the active sites [14,50].

As shown in Fig. 11, the catalytic cycle for the oxidation of ethanol to acetic acid involves the transfer of four electrons. This supposition is in full agreement with results of Jiang et al. [53], who showed that the electrooxidation of ethanol to acetate on Pd—Ni—P catalysts is a four-electron process. The titanium cations are not reduced in this process; however, the support material does influence the activity and lability of the oxygen atoms associated with vanadium. Although it is difficult to explain how O_2 molecules transform into lattice O^{2-} species on the monolayer V_2O_5/TiO_2 catalysts, the reoxidation of V^{3+} to V^{4+} and V^{5+} during the oxidation of ethanol was clearly demonstrated by XPS. Unfortunately, the experimental techniques used in this study do not allow us to elucidate the mechanism of reoxidation of reduced vanadia. Moreover, the reported results of quantum-chemical calculations of this process are sometimes rather controversial [44,54–56].

Hence, the oxidation of ethanol to acetaldehyde occurs at the redox V^{n+} sites via the redox Mars–van Krevelen mechanism [57] involving the reduction of V^{5+} to V^{4+} by ethanol and successive oxidation of V^{4+} to V^{5+} by gas-phase oxygen. At high conversion or at high temperatures, acetaldehyde can further oxidize to acetate species, also at the redox V^{n+} sites. In contrast, the oxidation of ethanol to acetic acid cannot be described by the classical Mars–van Krevelen mechanism. According to our reaction scheme (Fig. 11), the formation of acetic acid proceeds through at least two consecutive steps: the reduction of V^{5+} to V^{4+} and V^{3+} by ethanol with the formation of surface acetate species and the oxidation of vanadium cations by gas-phase oxygen simultaneously with desorption of acetic acid. Such a mechanism can be referred to as a modified Mars–van Krevelen mechanism. A similar mechanism has been proposed for the oxidation of formaldehyde to formic acid [58].

Finally, it should be noted that the mechanism for the oxidation of ethanol is complex, and some additional pathways for byproducts may be added to the proposed reaction scheme, but only after more detailed studies. For example, esterification of acetic acid with ethanol can result in small amounts of ethyl acetate; crotonaldehyde can form as a product of secondary reactions, such as aldol condensation of acetaldehyde; diethyl ether can form via the dehydration of ethanol on acidic sites. At the same time, some of these reactions cannot proceed over the monolayer vanadia–titania catalysts because the support surface is completely covered by the vanadia species, and adsorption of ethanol onto titania and the following spillover of intermediates are impossible. The influence of water on the product distribution was not considered, either. According to our previous studies [59], water drastically accelerates decomposition of formate and acetate species over vanadia–titania catalysts and can shift the oxidation of ethanol toward acetic acid.

5. Conclusions

The investigation reported here has provided preliminary insight into a detailed mechanism for the selective oxidation of ethanol to acetaldehyde and acetic acid over the monolayer V_2O_5/TiO_2 catalyst. Using in situ XPS and FTIR, we showed that the main surface intermediates are ethoxide species, adsorbed acetaldehyde, and acetate species. The selective oxidation of ethanol proceeds via the redox mechanism, where the oxidized catalyst surface oxidizes the reactant and is reoxidized by gas-phase oxygen. During the reaction, titanium cations remain in the Ti^{4+} state, whereas V^{5+} cations undergo reversible reduction to V^{4+} and V^{3+} under reaction conditions. Selective oxidation occurs through a series of successive stages. First, ethanol dehydrates to acetaldehyde, and then acetaldehyde transforms to acetic acid through the adsorbed acetate species. The formation and desorption of acetic acid occurs only in the presence of O_2 in the gas phase because the reduction of the catalyst stabilizes the surface acetate complexes.

Acknowledgments

This work was partially supported by the Ministry of Education and Science of the Russian Federation. The authors are grateful to G.Ya. Popova and E.V. Danilevich for conducting the catalytic tests and for fruitful discussions. The authors thank M. Hävecker, D. Teschner, R. Blume, R. Arrigo, T. Rocha, and M. Greiner for their assistance in carrying out the XPS experiments. The authors are also grateful to the staff of BESSY-II for their support during the beam time.

References

[1] A.V. Bridgwater, Biomass Bioenergy 38 (2012) 68.
[2] N. Koike, S. Hosokai, A. Takagaki, S. Nishimura, R. Kikuchi, K. Ebitani, Y. Suzuki, S.T. Oyama, J. Catal. 333 (2016) 115.
[3] T. Riittonen, V. Eta, S. Hyvärinen, L.J. Jönsson, J.P. Mikkola, Adv. Chem. Eng. 42 (2013) 1.
[4] B. Singh, A. Guldhe, I. Rawat, F. Bux, Renew. Sustain. Energy Rev. 29 (2014) 216.
[5] J. Scalbert, F. Thibault-Starzyk, R. Jacquot, D. Morvan, F. Meunier, J. Catal. 311 (2014) 28.
[6] B.A. Raich, H.C. Foley, Ind. Eng. Chem. Res. 37 (1998) 3888.
[7] X. Li, E. Iglesia, Chem. Eur. J. 13 (2007) 9324.
[8] B. Jorgensen, S.B. Kristensen, A.J. Kunov-Kruse, R. Fehrmann, C.H. Christensen, A. Riisager, Top. Catal. 52 (2009) 253.
[9] T. Takei, N. Iguchi, M. Haruta, Catal. Surv. Asia 15 (2011) 80.
[10] B. Mehlomakulu, T.T.N. Nguyen, P. Delichere, E. van Steen, J.M.M. Millet, J. Catal. 289 (2012) 1.
[11] Y.Y. Gorbanev, S. Kegnæs, C.W. Hanning, T.W. Hansen, A. Riisager, ACS Catal. 2 (2012) 604.
[12] T. Riittonen, K. Eränen, P. Mäki-Arvela, A. Shchukarev, A.-R. Rautio, K. Kordas, N. Kumar, T. Salmi, J.-P. Mikkola, Renew. Energy 74 (2015) 369.
[13] A. Knop-Gericke, E. Kleimenov, M. Hävecker, R. Blume, D. Teschner, S. Zafeiratos, R. Schlögl, V.I. Bukhtiyarov, V.V. Kaichev, I.P. Prosvirin, A.I. Nizovskii, H. Bluhm, A. Barinov, P. Dudin, M. Kiskinova, Adv. Catal. 52 (2009) 213.
[14] V.V. Kaichev, G.Ya. Popova, Yu.A. Chesalov, A.A. Saraev, D.Y. Zemlyanov, S.A. Beloshapkin, A. Knop-Gericke, R. Schlögl, T.V. Andrushkevich, V.I. Bukhtiyarov, J. Catal. 311 (2014) 59.
[15] E.V. Danilevich, G.Ya. Popova, T.V. Andrushkevich, V.V. Kaichev, Yu.A. Chesalov, V.A. Rogov, V.I. Bukhtiyarov, V.N. Parmon, Appl. Catal. A 475 (2014) 98.
[16] G.C. Bond, J.P. Zurita, S. Flamerz, P.J. Gellings, H. Bosch, J.G. van Ommen, B.J. Kip, Appl. Catal. 22 (1986) 361.
[17] G.C. Bond, S.F. Tahir, Appl. Catal. 71 (1991) 1.
[18] I.E. Wachs, Catal. Today 27 (1996) 437.
[19] I.E. Wachs, B.M. Weckhuysen, Appl. Catal. A 157 (1997) 67.
[20] B. Grzybowska-Swierkosz, Appl. Catal. A 157 (1997) 263.
[21] D.A. Bulushev, L. Kiwi-Minsker, F. Rainone, A. Renken, J. Catal. 205 (2002) 115.
[22] G.Y. Popova, T.V. Andrushkevich, E.V. Semionova, Yu.A. Chesalov, L.S. Dovlitova, V.A. Rogov, V.N. Parmon, J. Mol. Catal. A 283 (2008) 146.
[23] E.V. Ovchinnikova, T.V. Andrushkevich, G.Y. Popova, V.D. Meshcheryakov, V.A. Chumachenko, Chem. Eng. J. 154 (2009) 60.
[24] J.M. Coronado, K. Kataoka, I. Tejedor-Tejedor, M.A. Anderson, J. Catal. 219 (2003) 219.
[25] Z. Yu, S.S.C. Chuang, J. Catal. 246 (2007) 118.
[26] M. Li, Z. Wu, S.H. Overbury, J. Catal. 306 (2013) 164.
[27] R.G.J. Greenler, Chem. Phys. 37 (1962) 2094.
[28] A.M. Nadeem, G.I.N. Waterhouse, H. Idriss, Catal. Today 182 (2012) 16.
[29] V.S. Escribano, G. Busca, V. Lorenzelli, J. Phys. Chem. 94 (1990) 8945.
[30] V. Locar, H. Drobna, Appl. Catal. A 269 (2004) 27.
[31] H. Zhao, S. Bennici, J. Cai, J. Shen, A. Auroux, Catal. Today 152 (2010) 70.
[32] M. Sambi, G. Sangiovanni, G. Granozzi, F. Parmigiani, Phys. Rev. B 55 (1997) 7850.
[33] M.E. Harlin, V.M. Niemi, A.O.I. Krause, J. Catal. 195 (2000) 67.
[34] K.V.R. Chary, G. Kishan, C.P. Kumar, G.V. Sagar, J.W. Niemantsverdriet, Appl. Catal. A 245 (2003) 303.

[35] L.K. Boudali, A. Ghorbel, P. Grage, F. Figueras, Appl. Catal. B 59 (2005) 105.
[36] Z. Wu, F. Dong, Y. Liu, H. Wang, Catal. Commun. 11 (2009) 82.
[37] R.P. Holroyd, R.A. Bennett, I.Z. Jones, M. Bowker, J. Chem. Phys. 110 (1999) 8703.
[38] J.H. Kong, Y.K. Kim, Bull. Korean Chem. Soc. 32 (2011) 2531.
[39] P.M. Jayaweera, E.L. Quah, H. Idriss, J. Phys. Chem. C 111 (2007) 1764.
[40] V.V. Kaichev, V.I. Bukhtiyarov, G. Rupprechter, H.-J. Freund, Kinet. Catal. 46 (2005) 269.
[41] V.V. Kaichev, A.V. Miller, I.P. Prosvirin, V.I. Bukhtiyarov, Surf. Sci. 606 (2012) 420.
[42] A.V. Miller, V.V. Kaichev, I.P. Prosvirin, V.I. Bukhtiyarov, J. Phys. Chem. C 117 (2013) 8189.
[43] V.V. Kaichev, G.Ya. Popova, Yu.A. Chesalov, A.A. Saraev, T.V. Andrushkevich, V.I. Bukhtiyarov, Kinet. Catal. 57 (2016) 82.
[44] A. Goodrow, A.T. Bell, J. Phys. Chem. C 111 (2007) 14753.
[45] V. Shapovalov, T. Fievez, A.T. Bell, J. Phys. Chem. C 116 (2012) 18728.
[46] B.M. Weckhuysen, D.E. Keller, Catal. Today 78 (2003) 25.
[47] B. Beck, M. Harth, N.G. Hamilton, C. Carrero, J.J. Uhlrich, A. Trunschke, S. Shaikhutdinov, H. Schubert, H.-J. Freund, R. Schlögl, J. Sauer, R. Schomacker, J. Catal. 296 (2012) 120.
[48] B. Kilos, A.T. Bell, E. Iglesia, J. Phys. Chem. C 113 (2009) 2830.
[49] S.T. Oyama, W. Zhang, J. Am. Chem. Soc. 118 (1996) 7173.
[50] J. Döbler, M. Pritzsche, J. Sauer, J. Am. Chem. Soc. 127 (2005) 10861.
[51] V. Lorenzelli, G. Busca, N. Sheppard, J. Catal. 66 (1980) 28.
[52] V.I. Avdeev, V.N. Parmon, J. Phys. Chem. C 113 (2009) 2873.
[53] R. Jiang, D.T. Tran, J.P. McClure, D. Chu, ACS Catal. 4 (2014) 2577.
[54] X. Ding, W. Xue, Y. Ma, Y. Zhao, X. Wu, S. He, J. Phys. Chem. C 114 (2010) 3161.
[55] J.E. Molinari, I.E. Wachs, J. Am. Chem. Soc. 132 (2010) 12559.
[56] V.I. Avdeev, A.F. Bedilo, J. Phys. Chem. C 117 (2013) 14701.
[57] P. Mars, D.W. van Krevelen, Chem. Eng. Sci. 3 (1954) 41.
[58] G.Ya. Popova, T.V. Andrushkevich, Yu.A. Chesalov, V.N. Parmon, J. Mol. Catal. A 268 (2007) 251.
[59] G.Ya. Popova, Yu.A. Chesalov, E.M. Sadovskaya, T.V. Andrushkevich, J. Mol. Catal. A 357 (2012) 148.